INTERNATIONAL DESIGN CONFERENCE - DESIGN 2022
https://doi.org/10.1017/pds.2022.125

# Computational Design of an Additively Manufactured Origami-Based Hand Orthosis

M. O. Barros, A. Walker and T. Stanković ✉

ETH Zurich, Switzerland

✉ tinos@ethz.ch

**Abstract**

This work investigates the application of origami as the underlying principle to realize a novel 3D printed hand orthosis design. Due to the special property of some origami to become rigid when forming a closed surface, the orthosis can be printed flat to alleviate the most of the post-processing, and at the same time provide rigid support for the immobilized limb in the folded state. The contributions are the origami-based hand orthosis design and corresponding computational design method, as well as lessons learned regarding the application of origami for the hand orthosis design.

*Keywords: hand orthosis, origami-based design, additive manufacturing, computational design methods, biomedical design*

## 1. Introduction

The application of 3D printing, scanning, and advanced computational modeling to design hand orthoses for improved performance has received significant attention in recent years (Kim and Jeong 2015; Lin et al. 2016; Chen et al. 2017; De Souza et al. 2017; Li and Tanaka 2018a, 2018b). Although the conventional plaster casting procedure to immobilize upper limbs is a fairly simple process, the casts are relatively heavy, non-removable, and unventilated structures (Kim and Jeong 2015). Motivated by the fabrication possibilities of additive manufacturing (AM), researchers have proposed new AM-based designs to overcome the issues encountered with conventional casts. Most often, these designs are characterized by repetitive geometrical patterns to create removable, lightweight, and highly ventilated orthoses that, due to the best fit concept, reduce pressure points that may occur with conventional plaster casts (Kim and Jeong 2015; Lin et al. 2016; De Souza et al. 2017; Chen et al. 2017; Li and Tanaka 2018a, 2018b). These advantages lead to improved rehabilitation and fewer complications, such as minimized distortion during the healing process and a reduced infection risk, overall resulting in a higher patient satisfaction (Lin et al. 2016; Chen et al. 2017; Li and Tanaka 2018a, 2018b). However, there are downsides and challenges to 3D-printed designs. The fabrication requires a lot of support material resulting in long printing times and post-processing that includes mechanical grinding or rolling sharp edges, and removal of the support material using acid baths. In some cases, the post-processing also includes padding the cast and adding fixation components (Chen et al. 2017). The relevant literature reports some of the post-processing issues being addressed by proposing a hybrid approach (Kim and Jeong 2015), where an outer cover of a cast is produced in advance by injection molding, or to design and fabricate an orthosis in a flat state that needs to be heated up to allow plastic deformation and fitting to the patient's limb (De Souza et al. 2017).

In response to the challenges and opportunities of designing personalized hand orthoses for AM and improved rehabilitation, this work investigates the application of origami as the underlying principle to realize a novel hand orthosis design. Due to its ability to transform a flat sheet into almost any, origami

receives significant attention from scientist and design practitioners alike as an inspiration for the design of novel applications across many scientific and engineering domains (Meloni et al. 2021). Here, origami principles are used to design an origami-based hand orthosis customizable to the shape of a patient's arm. Since the origami-based orthosis is fabricated flat and then folded to the required shape, the printing time is reduced and much of the additional post-processing is alleviated in comparison to the related designs. Another motivation for origami stems from the fact that certain patterns, once they form a closed surface, become load-carrying, which in the case of a hand orthosis design is a beneficial characteristic that provides support and fixation for the immobilized limb. The contributions of this work are the origami-based hand orthosis design and a computational method to generate patient-specific designs, as well as lessons learned regarding the application of origami and multi-material AM in the context of the hand orthosis design.
The paper is organized as follows: First, the background section reviews related work on hand orthosis design, origami-based design, and draws the motivation for this work. Then, the method section introduces the computational method for the design of an origami-based hand orthosis involving the hand orthosis design. Subsequent to the method section, are the results, and the discussion section. The conclusion section summarizes the main takeaways of this work.

## 2. Background

The Background first focuses on the relevant work in AM design alternatives to plaster casts. The second section discusses origami-based design in context of this work by briefly explaining what origami is and presents known crease patterns that can be used for the hand orthosis design, as well as an overview of the existing origami embodiment approaches. The last section gives the motivation for this work.

### 2.1. Design of Hand Orthoses for Improved Rehabilitation

In their work, Li and Tanaka (2018a, 2018b) use patient specific data acquired through scanning, and develop a parametric model of a personalized hand orthosis for AM. Their approach results in a two-component shell orthosis that is fixated with four screws. The approach from Lin et al. (2016) generates a surface pattern and a solid model of a cast based on the image-based patient data and using a commercial Computer-Aided Design (CAD) software. Their approach allows medical technicians with little CAD experience to interface with the scanned anatomic mesh, build an orthosis model, and export the fabrication data. In a subsequent paper, their approach is applied to design a 3D-printed and patient-specific cast for the treatment of distal radius fractures (Chen et al. 2017). The results report a minimized distortion during the healing process and an increase in patient comfort due to personalized geometry. Furthermore, the ventilated structure featured in the novel cast reduces the risk of cutaneous complications. The post-processing includes padding, mechanical grinding or rolling sharp edges, and adding fixation components. Chen et al. (2017) conducted clinical trials with the focus on mild distal fractures reporting that the design and fabrication of AM-based orthoses requires more time in comparison to conventional plaster casting. The time difference is mainly due to the complex structures of AM orthoses, which results in a lot of support material. Despite its personalized structure and lightweight design, which improves patient experiences, solely 3D-printed orthoses are recommended not to be used in emergency situations of an acute fracture that require fast response times (Chen et al. 2017). To reduce the response times, Kim and Jeong (2015) proposed a hybrid manufacturing methodology that utilizes AM and injection molding. There, the two outer shells of an orthosis are produced by injection molding and are the same for each patient, whereas only the inner shell is 3D printed and patient-specific. To reduce the printing time even more, De Souza et al. (2017) propose a new methodology for generating orthoses for which a scan of the affected limb is not necessary. Instead, the required measurements to fit the orthosis to a patient are can be taken directly from the wrist. Based on these measurements, a predesigned pattern is scaled to the patient resulting in an orthosis that can be printed flat, which only took 45 minutes. During post-processing, the orthosis is heated up to be adapted to the patient.

### 2.2. Origami-Based Design

The application of origami for engineering applications can be broken down into two major directions, namely design approaches that draw the inspiration from origami-like geometry but otherwise show little resemblance to a behavior of an origami (Francis et al. 2014) and approaches that adapt the



https://doi.org/10.1017/pds.2022.125 Published online by Cambridge University Press

kinematics of origami (Zirbel et al. 2013) into new designs. Due to the complex kinematics of origami structures origami adaptation triggered significant research producing mathematical models of various patterns (Lang 2017), the development of computational approaches to assist origami-adaptation (Demaine and Tachi 2017; Dieleman et al. 2020; Zimmermann et al. 2020; Dudte et al. 2021; Yu et al. 2021; Zimmermann et al. 2021), as well as the development of approaches to accommodate for finite thickness of faces during the embodiment design phase (Lang et al. 2018).
Each origami is defined by its crease pattern, which comprises a set of edges, i.e. crease lines, alongside which the folding is performed, a set of vertices in which each vertex is defined by an intersection of at least two edges, and the folding directions that distinguish edges as a valley or a mountain crease. Figure 1a exemplifies this information by highlighting a portion of the traditional Waterbomb pattern (Chen et al. 2016) using round markers for vertices, and thick blue and red dashed lines for mountain and valley creases, respectively. Figure 1a also shows that each vertex not located on the edge of the paper, i.e. an internal vertex, is a degree 6 vertex, since it is connected to 6 creases. Patterns in Figures 1c and 1d are degree 6 vertex patterns. Figures 1b and 1e show degree 4 vertex patterns.

### *2.2.1. Candidate Crease Patterns Overview*

Here we asses a set of five known crease pattern (shown in Figure 1) that can fold into a tube-like configuration starting from a flat configuration, and could be used to design a hand orthosis.

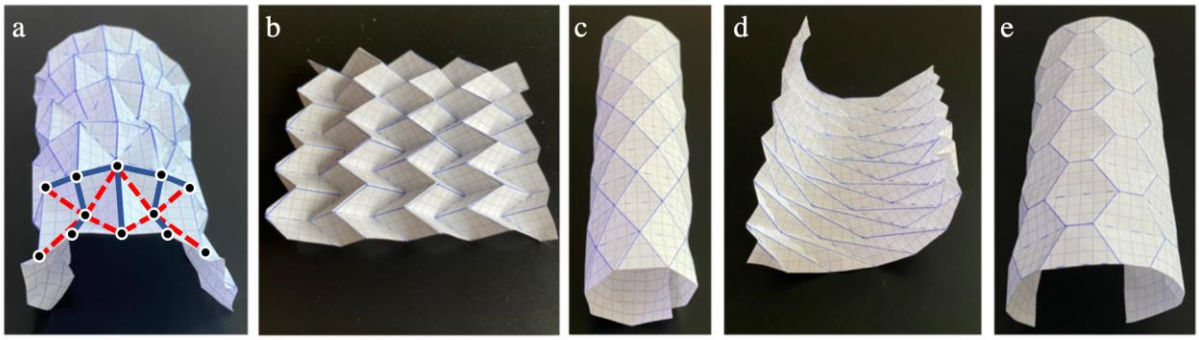


**Figure 1. Paper prototypes of origami crease patterns with tube-like folding configurations. Mountain and valley creases shown using continuous and dashed lines, respectively. Waterbomb pattern with partially highlighted vertices, mountain (thick blue lines) and valley creases (thick red dashed lines) (a), Miura-Ori pattern (b), Yoshimura pattern (c), Tilted-Yoshimura pattern (d), "Hexagonal"-Yoshimura pattern (e).**

The waterbomb pattern (Figure 1a) is a well-known origami built up from a base. that is then ordered such that always six crease lines meet at every vertex (Chen et al. 2016). Tang et al. (2012) proposed a method on how to approximate a surface of revolution using the waterbomb pattern. First, the surface of revolution is discretized, and a three-dimensional crease map is generated. Each quadratic base is then altered in a way to fit the generated crease map, resulting in folding surfaces of revolution that were convex, concave, or even both. The Miura-Ori pattern (Figure 2a) invented by Koryo Miura (1985) to fold maps into a configuration resembling a thickened plane, is one of the best known origami patterns. The folding into a thickened plane-like configuration was used by Dudte et al. (2016) to develop a computational approach in which rotationally symmetric surfaces are folded using the same pattern. The last pattern found in literature to fold into a tube is the Yoshimura pattern (Yoshimura 1951), here shown in Figure 1c-1e in three different variants. Unlike the patterns in Figures 1a and 1b, the cylinder with the Yoshimura pattern is a load-carrying structure, and thus cannot fold further without material strains, which means that once the pattern is folded, it locks and becomes a rigid structure (Cai et al. 2015), making it particularly suitable for the hand orthosis design.

### *2.2.2. Embodiment*

The review of thickness-accommodation techniques in origami-inspired engineering by Lang et al. (2018), proposes several techniques to thicken an origami (the membrane and strained joint techniques are shown in Figures 2a and 2b, respectively).



https://doi.org/10.1017/pds.2022.125 Published online by Cambridge University Press

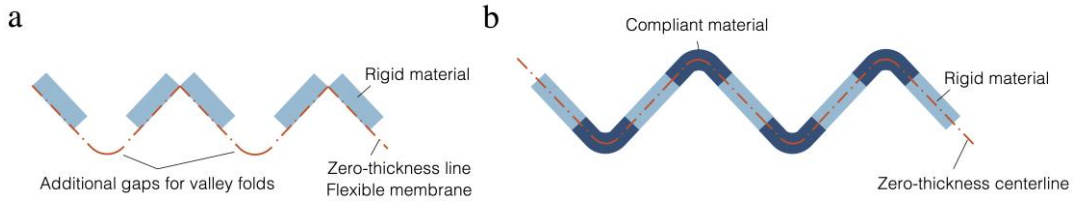


**Figure 2. Membrane (a) and strained joint (b) techniques for origami thickness accommodation. Based on Lang et al. (2018).**

Each technique addressed by Lang et. al. has a particular way of adding material to the crease line to get a foldable, thickened origami, and two or more approaches can also be combined to create a design-specific method to thicken a crease pattern. The choice of an approach depends on the origami configuration and application. The membrane technique and the strained joint technique could be used with multi-material AM to realize flexible and rigid elements of an origami with finite thickness. Other approaches proposed by Lang et al. require hinges, which depending on the crease pattern dimensions could end up being too small to realize using AM.

### 2.3. Implications for this Work

The review of the approaches to design novel hand orthoses for improved rehabilitation shows that the orthosis designs are lightweight, ventilated, removable and personalized. It is also shown that the predominant fabrication method in realizing these designs is AM, which was also found in a combination with other manufacturing methods. Out of the two techniques in Figure 2 that can be easily realized using multi-material printing, the concept of strained joint technique was chosen to embody the hand orthosis, since the membrane technique leads to gaps between rigid faces that will ultimately reduce the overall stiffness of the orthosis.

Origami folding is characterized by a complex folding motion for which it is difficult to calculate a shape approximating configuration based on the starting configuration for an arbitrary crease pattern. To avoid this, the computational method proposed in this work will undertake an inverse design strategy that directly calculates the origami-based hand orthosis in the folded state and adapts it to the scanned arm. To reduce the search space of possible alternatives and make the inverse design strategy possible, a Yoshimura-based pattern is selected as a foundation for the parametric hand orthosis model, since once folded, it becomes a rigid structure providing the necessary support for the affected limb. In particular, the pattern in Figure 1c is selected as the most suitable of the three load-carrying variants. To clarify, the pattern in Figure 1e adds an additional complication to the orthosis design due to its tilted valley crease lines producing stripes of triangles not horizontal with respect to the base of the tube. Such design is more difficult to parametrize in comparison to the patterns in Figures 1c and 1e with valley crease lines parallel to the tube base. For the patterns in Figures 1c and 1e, it is visible that the Yoshimura pattern has vertices of degree 6, while the Hexagon-Yoshimura has vertices of degree 4. These additional degrees lead to additional degrees of design freedom, which can be explored to design the parametrization of the pattern such that it can be personalized.

The next section proposes a computational method for the design of origami-based hand orthoses based on the Yoshimura pattern. The orthosis is fabricated using AM and embodied using the strained joint technique.

## 3. Method

The proposed workflow for the design and fabrication of an origami-based hand orthosis consists of three phases as shown in Figure 3. Phase 1 involves the data acquisition with scanning and post-processing, and the shape approximation of a scanned arm using a set of ellipses $\mathbb{E}$. Phase 2 designs the personalized crease pattern in the folded state based on the modifications of Yoshimura pattern and a subset of preselected ellipses $\mathbb{S}$ in $\mathbb{E}$ that define a set of cross-sectional cuts around which the crease pattern will be generated. The fabrication with embodiment is performed in Phase 3.



https://doi.org/10.1017/pds.2022.125 Published online by Cambridge University Press

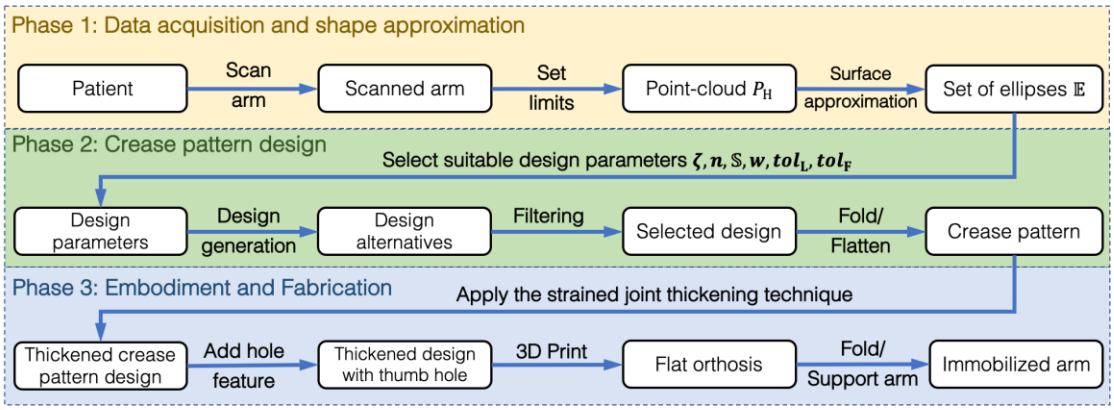


**Figure 3. Computational method for the design of an origami-based hand orthosis.**

## 3.1. Data Acquisition and Surface Approximation

After the scanning is performed (here the smartphone app Qlone is used, (Qlone 2021)), the resulting point cloud is first subject to a limit setting procedure in which points that the orthosis will not consider are removed, involving the removal of thumb and the fingers using two manually defined planes (Figure 4a), and using a third plane that to make a horizontal cut to define the base of the orthosis.

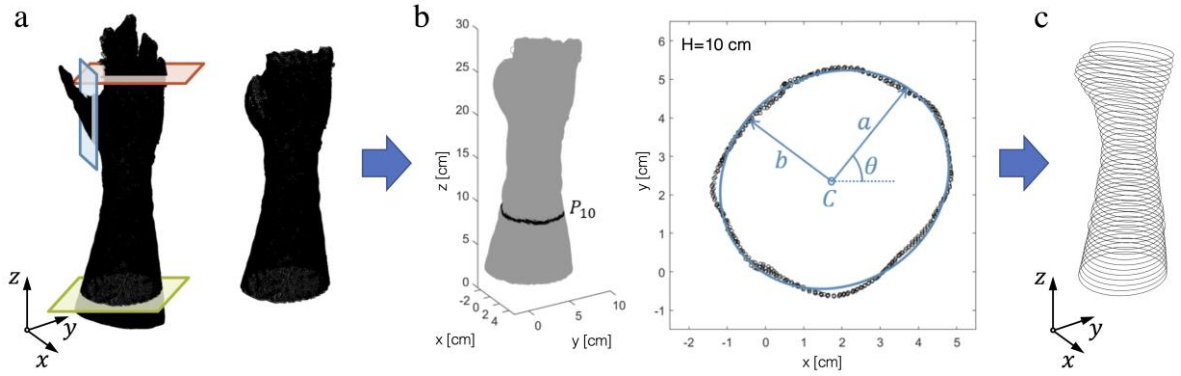


**Figure 4. Data acquisition process. Manual removal of the points in the point cloud that the orthosis will not cover (a). Parametric model using an ellipse to approximate the point cloud given the cutting height (b). Approximation of the point-cloud using a set of ellipses (c).**

To mathematically describe the outside surface of the point cloud, a set of ellipses $\mathbb{E}$ (Figure 4b and 4c) is used. Every ellipse in $\mathbb{E}$ is defined by a center point $\vec{C} \in \mathbb{R}^3$, a planar rotation angle θ, two semi-axes $a$ and $b$, and a cutting height defining the elevation of a plane carrying an ellipse:

$$z = H \tag{1}$$

Each cutting plane is parallel to the $xy$-plane and $h = 5$ mm apart. The set of points $P_H$ that are approximated with each ellipse is obtained by the following expression:

$$P_H = \{(x, y, z) \in \mathbb{R}^3 \mid H - 2\text{mm} \leq z \leq H + 2\text{mm}\} \tag{2}$$

The points $\vec{j}$ in the set $P_H$ are taken from a reasonable range of $\pm 2$ mm and vertically projected to the cutting plane $z = H$. The optimization problem in Equation 3 is solved to obtain an ellipse from a set of points $P_H$ at $\vec{C}\big|_z = \text{H}$ in terms of $\vec{C}$, θ, a, and b by minimizing the squared sum of the distance from each point $\vec{j} \in P_H$ to the ellipse:

$$\min_{\vec{C},\theta,a,b} \sum_{\vec{j}\in P_H} (\|\vec{j} - \vec{r}(\phi)\|)^\rho$$

$$s.t. \ \min_{\vec{j}\in P_H} \vec{j}|_x \leq \vec{C}\big|_x \leq \max_{\vec{j}\in P_H} \vec{j}|_x, \min_{\vec{j}\in P_H} \vec{j}|_y \leq \vec{C}\big|_y \leq \max_{\vec{j}\in P_H} \vec{j}|_y, \vec{C}\big|_z = H \tag{3}$$



https://doi.org/10.1017/pds.2022.125 Published online by Cambridge University Press

$$0 \le a \le \sqrt{\max_{\vec{j}\in P_H}|\vec{j}|_x|^2 + \max_{\vec{j}\in P_H}|\vec{j}|_y|^2},\ 0 \le b \le \sqrt{\max_{\vec{j}\in P_H}|\vec{j}|_x|^2 + \max_{\vec{j}\in P_H}|\vec{j}|_y|^2},\ 0 \le \theta \le \pi$$

where the ellipse $\vec{r}(\phi)$ is parametrized in terms of the polar angle $\phi$ using the following equation:

$$\vec{r}(\phi) = \left( \begin{pmatrix} a \cdot \cos(\phi) \\ b \cdot \sin(\phi) \\ 0 \end{pmatrix} + \vec{C} \right) \cdot \begin{bmatrix} \cos\theta & -\sin\theta & 0 \\ \sin\theta & \cos\theta & 0 \\ 0 & 0 & 1 \end{bmatrix}, \qquad \phi \in [0, 2\pi] \tag{4}$$

The parameter $\rho$ is set to $\rho = 2$ to increase the convergence of the problem in Equation 3. The distance from each point $\vec{j} \in P_H$ to the ellipse in the objective of Equation 3 is calculated by increasing $\phi$ incrementally from 0 to $2\pi$ and taking the smallest value. The boundary conditions in Equation 3 ensure that the ellipse centre $\vec{C}$, as well as the semi-axes lay within the point cloud. Equation 3 is solved using the interior-point algorithm in MATLAB with the stopping condition step tolerance of 1e-3.

## 3.2. Crease Pattern Design

The Yoshimura pattern consists (Figure 5a) of several rows of rhombi composed of two triangles stacked on top of each other and delimited by a horizontal valley fold. Here, the pattern is defined by the positions of vertices $P_{c,i}$ of each triangle, where index $c$ corresponds to an ellipse $e_c$ in $\mathbb{S} \subseteq \mathbb{E}$, and $i$ indexes the vertices of a surrounding polygon enveloping the corresponding ellipse $e_c$ (Figure 5b).

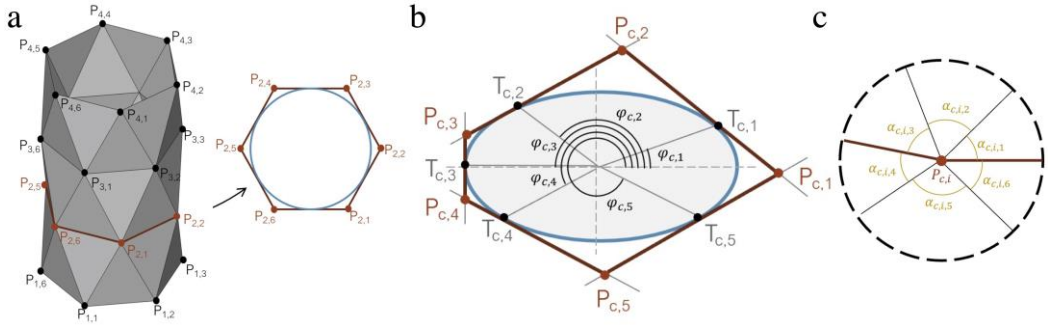


**Figure 5. A folded Yoshimura pattern with $P_{c,i}$ shown (a), parametrization of the surrounding polygon (b), indexing of the sector angles $\alpha_{c,i,k}$ for an internal vertex $P_{c,i}$ (c).**

To calculate the vertices $P_{c,i}$, first a coordinate transformation (denoted using $'$) is performed such that the origin $\overrightarrow{C_c}$ of each ellipse is translated to $(0, 0, H)$ with semi-axes $a$ and $b$ aligned with coordinate axes $x$ and $y$, respectively. The vertices $P'_{c,i}$ of the surrounding polygon in the transformed coordinates are equal to the intersection of the tangents on the ellipse (Figure 5b) and can be calculated given a vector containing the polar angles $\varphi_{c,i}$ and the polygon degree $n$:

$$P'_{c,i} = T'_{c,i} + \frac{\cos(\varphi_{c,i} - \varphi_{c,l})}{\sin(\varphi_{c,i} - \varphi_{c,l})} \cdot \begin{pmatrix} -a_c \cdot \sin(\varphi_{c,i}) \\ b_c \cdot \cos(\varphi_{c,i}) \\ 0 \end{pmatrix}, \qquad l = \begin{cases} i+1, & i < n \\ 1, & i = n \end{cases} \tag{6}$$

Where $T'_{c,i}$ are the tangent points on the ellipse $e_c$ in the transformed coordinates:

$$T'_{c,i} = \begin{pmatrix} a_c \cdot \cos(\varphi_{c,i}) \\ b_c \cdot \sin(\varphi_{c,i}) \\ 0 \end{pmatrix} \tag{7}$$

The location of the transformed vertices $P_{c,i}$ in the original coordinates is found after applying the rotation about $\theta_c$ and translation to the ellipse center $\overrightarrow{C_c}$, as described by the following equation:

$$P_{c,i} = \begin{bmatrix} \cos\theta_c & -\sin\theta_c & 0 \\ \sin\theta_c & \cos\theta_c & 0 \\ 0 & 0 & 1 \end{bmatrix} \cdot P'_{c,i} + \overrightarrow{C_c} \tag{8}$$



https://doi.org/10.1017/pds.2022.125 Published online by Cambridge University Press

The lengths of the polygon sides $L_{c,i}$ follow directly from the point coordinates $P_{c,i}$:

$$L_{c,i} = \begin{cases} \left|P_{c,i+1} - P_{c,i}\right|, & i < n \\ \left|P_{c,1} - P_{c,n}\right|, & i = n \end{cases} \tag{9}$$

Given the total number $\zeta$ of ellipses in the subset $\mathbb{S}$ (number of cuts) and the polygon degree $n$, the vertices $P_{c,i}$ can be found by optimizing the surrounding polygon in terms of $\varphi_{c,i}$ at each cut such that it envelops the corresponding ellipse $e_c$ with the smallest area (Equations 10a-10e):

$$\min_{\vec{\varphi}} \sum_{c=1}^{\zeta} \left(\text{area}(polygon_c) - \text{area}(e_c)\right)^2 \tag{10a}$$

$$s.t.\ \text{area}(polygon_c) - \text{area}(e_c) \leq 0 \tag{10b}$$

$$w(1) \cdot \max\{0,\ tol_{\text{L}} - L_{c,i}\} = 0 \tag{10c}$$

$$w(2) \cdot \max\{0,\ \left|2\pi - \sum_{k=1}^{6} \alpha_{c,i,k}\right| - tol_{\text{F}}\} = 0 \tag{10d}$$

$$0 \leq \varphi_{c,i} \leq 360°, \quad \forall\, c \in [1, \zeta], i \in [1, n] \tag{10e}$$

where the equality constraints in Equations 10c and 10d are implemented using a two-valued vector of weights $\vec{w}$ in which $w(1)$ scales the violation of length $L_{c,i}$ of each polygon sides with respect to the lowest allowable edge length $tol_{\text{L}}$, and $w(2)$ scales the developability of the pattern with respect to some small value $tol_{\text{F}}$. The developability of a crease pattern in Equation 10d is given by the condition that the sector angles $\alpha_{c,i,k}$ at each internal vertex sum up to 360° (Lang 2017) (Figure 5c). The sector angles $\alpha_{c,i,k}$ are calculated using the law of cosines. The formulation of the constraints in Equations 10c and 10d as equality constraints and using the max function are based on pre-testing in which inequality-based formulations performed poorly. The optimization is solved using the interior-point algorithm in MATLAB with the number of function evaluation limited to $300 \cdot \zeta$.

## 3.3. Embodiment and Fabrication

First, an additional row of triangles is added to the pattern in flat configuration (see Figure 6a) to generate two overlapping rows that ensure the closing of the orthosis in folded configuration. Using the strained joint thickness technique, the pattern is thickened to the outer side of the arm according to Figure 6b since the crease line of the folded configuration lies on the arm. The width of the crease lines as well as the height of the crease pattern are both set to 3 mm.

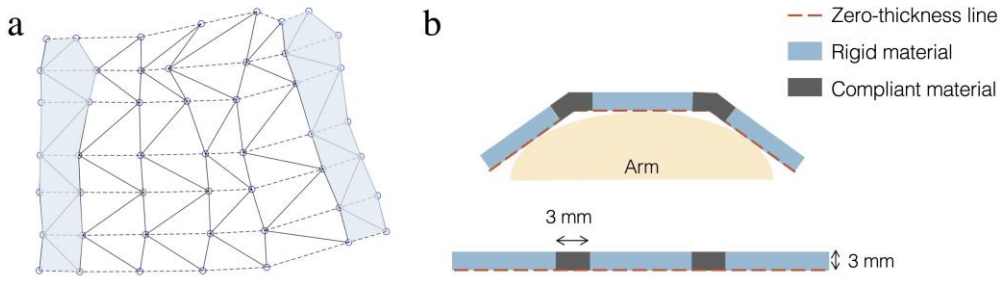


**Figure 6. Adding the additional overlapping row to ensure the closing of the orthosis (a), thickness accommodation based on modified strained joint technique (b).**

The fabrication is performed using a Polyjet based multi-material 3D printer Objet500 Connex from Stratasys. The rigid faces are fabricated using the VeroWhitePlus material and the compliant crease lines using the rubber like material Agilus30Black. The orthosis is printed flat with no support structures.



https://doi.org/10.1017/pds.2022.125 Published online by Cambridge University Press

# 4. Results

The section starts with the results of the surface approximation using ellipses. Afterwards, the results for the crease pattern design are presented, involving the determination of design parameters that lead to usable orthosis designs. Lastly, the produced prototype is presented.

## 4.1. Surface Approximation Results

The point cloud is approximated with a set containing 45 ellipses (Figure 7a). The base plane for the approximation is set at $H = 3$ cm and the last plane is at $H = 25$ cm. Figure 7a shows examples of four cuts at different heights approximated by different ellipses.

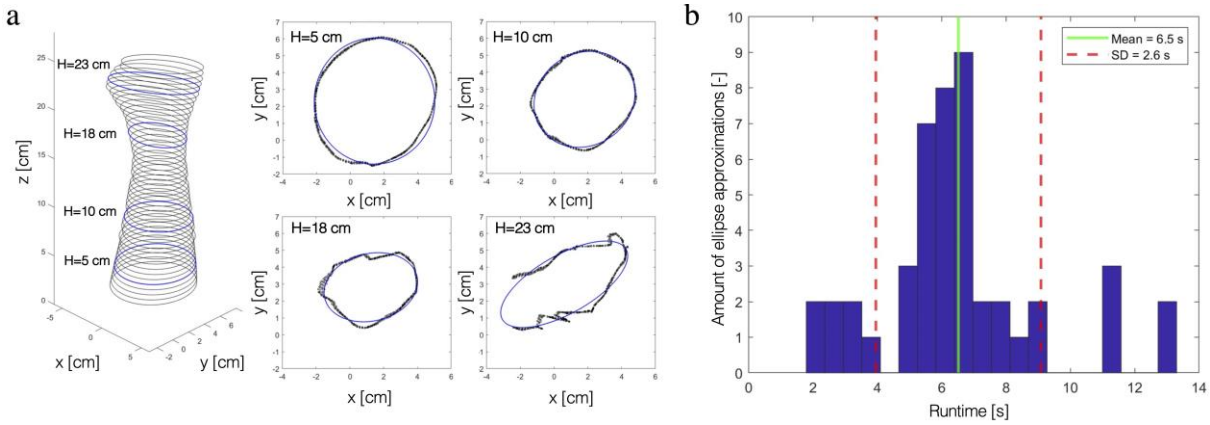


**Figure 7. Surface approximation using ellipses with four cuts at different heights (a). Histogram of the runtimes of all ellipse approximations (b).**

A histogram of the runtimes of all ellipse approximations is shown in Figure 7b. The mean runtime for an ellipse approximation is 6.5 s with a standard deviation of 2.6 s. The generation of the entire set took 4 min 59.9 s. The ellipse at $H = 23$ cm has points omitted due to the thumb removal (Figure 4a).

## 4.2. Crease Pattern Design Results and Prototyping

To find the range of parameters that lead to usable origami-based orthosis designs, the optimization problem in Equations 10a-10e is solved exhaustively for all possible parameter settings. The exhaustive search is performed on the high-performance computing cluster Euler at ETHZ. Table 1 states the possible parameter values based on an initial guess. The usable range of parameters, once determined, will serve as a design heuristic to be used by clinicians without the need to do the exhaustive search.

**Table 1. Overview of the design parameters and their ranges for the exhaustive search**

| Variable | Definition | Design parameter settings |
|---|---|---|
| $\zeta$ | Number of ellipses used to generate the hand-orthosis | 5, 6, 7, 8 |
| $\mathbb{S}$ | A subset containing $\zeta$ ellipses from $\mathbb{E}$ | All possible subsets such that any two ellipses are at least 3 cm apart |
| $n$ | Polygon degree | 5, 6, 7 |
| $\vec{w}$ | Vector of penalty weights | (1, 1) or (10, 1) |
| $tol_{\mathrm{L}}$ | Tolerance on edge lengths | 2 cm |
| $tol_{\mathrm{F}}$ | Tolerance on developability | 1° |

The number of ellipses $\zeta$ used to generate the hand-orthosis considers all possible subsets in $\mathbb{E}$ that fulfill the condition that two ellipses are at least 3 cm apart from each other to avoid polygons with a small height. Figure 8a shows how many subsets $\mathbb{S}$ could be generated for each chosen value of $\zeta$, after which an exhaustive search is performed over all possible combinations of the remaining design parameters



https://doi.org/10.1017/pds.2022.125 Published online by Cambridge University Press

using Equation 10. For the penalty weights, only two options are considered. While the first set of weights has no preferences to length and developability constraints, the second set weighs the length constraint 10 times higher than the developability constraint.

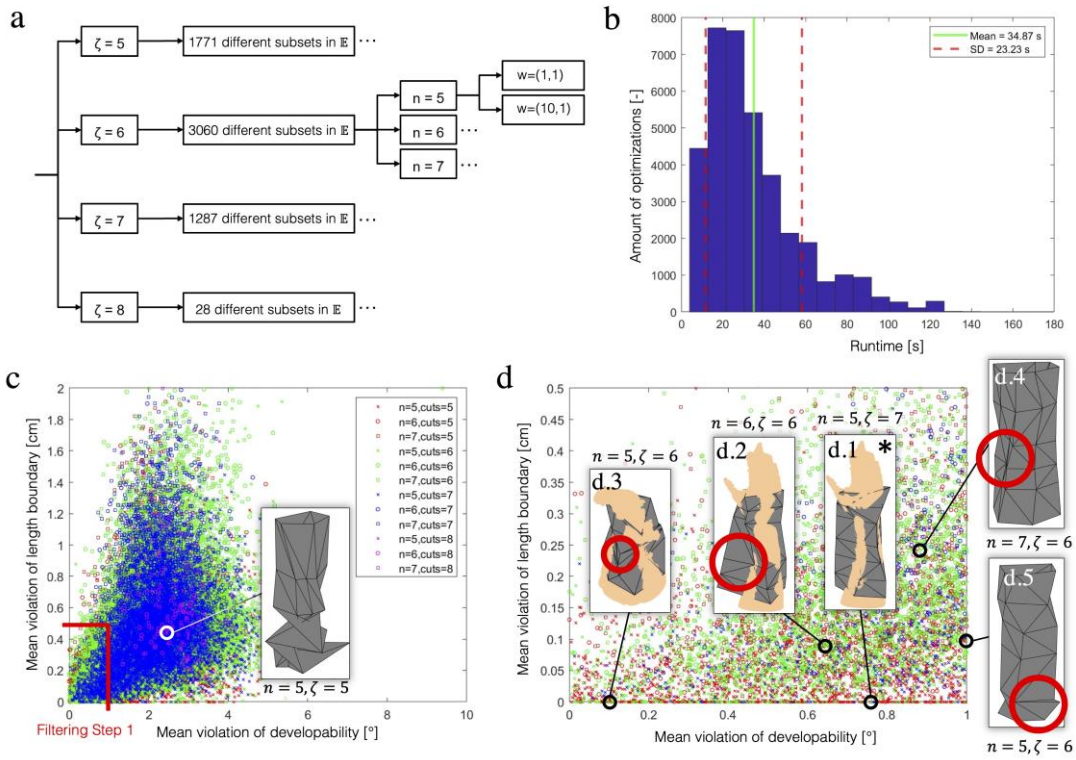


**Figure 8. Design parameters determination scheme (a). Histogram of the runtimes of optimizations using Equation 10 (b). Design search space in terms of the polygon degree $n$ and number of cuts $\zeta$ with respect to the mean length boundary and developability violations (c). Design search space filtering resulting in 682 possible designs (d).**

The exhaustive search generated 36'876 designs based on different optimization parameters. The histogram of the optimization runtimes in Figure 8b shows the mean runtime value of 34.87 s and a standard deviation of 23.23 s. The distribution of the generated designs with respect to the mean violation of the developability and the length boundary are shown in Figures 8c. To identify the usable set of design parameters, the designs are first filtered based on their constraint violations in which the mean violation of the length boundary and developability is limited to 0.5 mm and 1°, respectively (see Figure 8c Filtering Step 1). The 0.5 mm value for the length boundary is determined to account for the worst-case constraint violation that would still guarantee edge lengths of 1.5 cm. The narrow 1° violation for developability is defined based on the severity the developability has on the designs' usability.

The filtering process reduced the design space to 632 possible designs in total, where 489 designs have five cuts, 125 designs have six cuts and 18 designs have seven cuts (Figure 8d). Further examination of the results filtered out designs with five cuts due to the inaccuracy of the surface approximation. An example of a design with five cuts featuring a large twist and an intersection of faces is shown as a detail in Figure 8c (the subset $\mathbb{S}$ of ellipses at heights {3, 6, 11, 16.5, 25} [cm] and weight factors (10, 1)). The remaining 143 designs are inspected manually until only one design remains. The chosen design (shown in Figure 8d.1 and Figure 9a) consists of seven cuts and a polygon degree five, the subset $\mathbb{S}$ of ellipses at heights {3, 6.5, 10.5, 14, 19, 22, 25} [cm], and weight factors (10, 1). The design in Figure 9d.2 $n = 6,\ \zeta = 6,\ \mathbb{S} \in$ {3, 6, 10, 19, 22, 25} [cm], weight factors (10, 1), performs better with respect to developability but worse considering edge length in comparison to the best design due to the edges that are too long. The design located closer to (0, 0) point, Figure 8d.3 ($n = 5,\ \zeta = 6,\ \mathbb{S} \in$ {3, 10, 13.5, 17.5, 21, 25} [cm], weight factors (10, 1)) and rotated for better view have superior surface approximation than the best design, but the design involves spikes that significantly impair the comfort and do not



https://doi.org/10.1017/pds.2022.125 Published online by Cambridge University Press

conform to the surface of the arm. The designs that perform worse in comparison to the best design are exemplified in Figures 8d.4 $n = 7,\ \zeta = 6,\ \mathbb{S} \in \{3, 8, 11, 14.5, 19.5, 25\}$ [cm], weight factors (1, 1), and 8d.5 $n = 5,\ \zeta = 6,\ \mathbb{S} \in \{3, 6, 12.5, 16.5, 20.5, 25\}$ [cm], weight factors (10, 1), showing concave regions, or twists, respectively. The 3D printed orthosis prototype in the folded and flat states are shown in Figures 9b and 9c, respectively. In the current design, the two columns that are overlayed are being held manually together. The fabricated orthosis also includes a hole for the thumb feature, which is added manually to the crease pattern before printing.

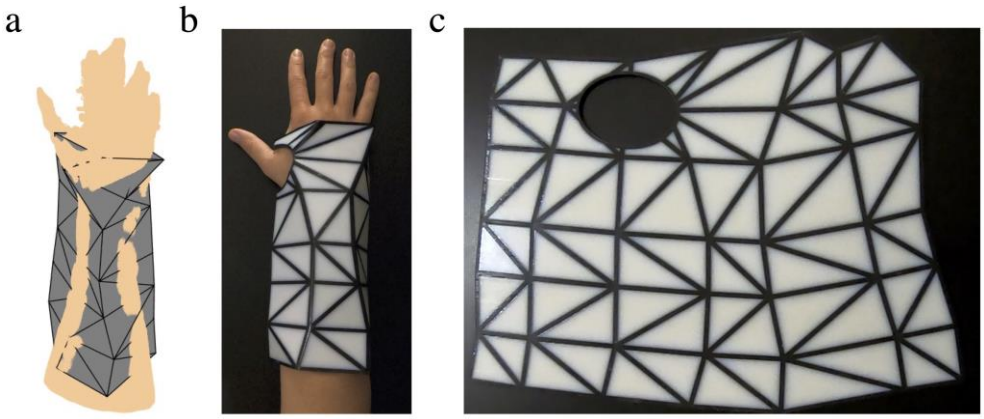


**Figure 9. Final hand-orthosis crease pattern design with 7 cuts and a polygon degree 5 (a). Top view on 3D printed orthosis prototype in the folded (b) and flat (c) states. The printing process took 1 h and 46 min. The prototype weighs 237 g and includes a hole for the thumb feature.**

## 5. Discussion

The section focuses on the results interpretation by discussing the implications for the design of hand-Orthosis, algorithmic performance, as well as outlining the limitations of this work.

### 5.1. Implications for the Design of Hand-Orthosis

The results show that better orthosis designs are produced if the number of cuts $\zeta$ tends towards higher values (given in Table 1), and when ellipses in $\mathbb{S}$ are distributed equidistantly (Figure 8d.1). In contrast, the design shown in a detail view in Figure 8c, as well the design in Figure 8d.2 exhibit an uneven distribution of $\mathbb{S}$ over the length of the limb that impairs their usability.

The designs with a smaller number of cuts $\zeta = 5, 6$ and polygons of degree $n = 5$ often result in twists or spikes, as exemplified in Figure 8d.5 and Figure 8d.3, respectively. The increase of the number of polygon sides $n$ can also result with negative effects by introduction of concave regions in the orthosis design (Figure 8d.4). The concave regions are produced by the optimization trying to pack a high number of polygon sides while trying at the same to enforce the minimum edge length of 2 cm.

The selected orthosis design (Figure 9a) shows some portions of the limb protruding the orthosis shape. The initial tests with the physical prototype (Figures 9b and 9c) indicated that this is not problematic since the arm is compressed while the orthosis is secured. However, what came as a difficulty is to position the orthosis around the arm such that the crease lines are at their intended locations. The wrong positioning causes gaps inside the orthosis, leading to a not fully immobilized wrist. The problem could be solved by making the orthosis thicker and then subtract the volume of scanned arm from the orthosis using a CAD system. After fabrication, the orthosis would allow ease in applying the orthosis and allow for the arm to fit better in the folded state.

### 5.2. Algorithmic Performance

The surface approximation can be improved by ensuring that the ellipse fully surrounds the point cloud by weighting the distances of the points inside the ellipse higher than the ones outside. This would contribute to fewer points to lay outside of the generated folded configuration. The improvement in the results could also be achieved by application of a better scanning procedure at the data acquisition step.



https://doi.org/10.1017/pds.2022.125 Published online by Cambridge University Press

The use of a CT scan or a photometric scanner (Lin et al. 2016) could improve the data by removing various uneven areas occurring in the point cloud of the scanned limb.
The histogram of the runtimes shown in Figure 8b shows that 85% of all generated patterns took less than one minute. Therefore, taking the mean of the ellipse approximation runtimes of 6.5 s (Figure 8a) together with the runtime for the crease-pattern design generation, it shows that the origami-based hand orthosis is designed relatively fast compared to the 3D-printed alternatives found in literature. However, the benefit of short runtimes is valid under the assumptions that the set of design parameters that lead to a feasible and manufacturable origami-based hand orthosis designs is known and that the filtering and exploration of the design space is automated. Whereas the former is partially tackled in this work, the latter requires a significant improvement and is left for future research.
Although the optimization in Equation 10 is solved efficiently, the problem not always yields feasible solutions. This also corroborates to the fact that the pre-testing using inequality constraint formulations for Equations 10c and 10d yielded longer runtimes with significantly worse solutions than reported here. Furthermore, the location of the chosen design in Figure 8d.1 in comparison with the more feasible but less usable design in Figure 8d.3 shows that more work is required to incorporate user requirements better into the design method.

### 5.3. Other Limitations

At this stage of the research the data acquisition is not varied over different subjects. Therefore, only one arm was scanned and parametrized. Thus, to prescribe a set of design parameters that accommodate the change in the anthropometric measures, a separate and more extensive empirical study is required.
During the prototyping it was noticed that some crease pattern edges started to crack only after a few trials. This is mainly due to the chosen materials and their mechanical properties. This suggests that the realization of the orthosis would require different martials, or even a different 3D printing process.

## 6. Conclusion

In this work, a novel origami-based hand orthosis design and a computational method to generate patient-specific designs are proposed. The proposed design is based on the Yoshimura pattern due to its property that once folded to a cylindrical-like shape it locks to a rigid structure, which is beneficial for arm immobilization. In comparison to AM orthosis designs reported in literature, the proposed design is advantageous since it can be fabricated flat (without support structures) using multi-material 3D printing, and folded to a shape conforming to the affected limb. Despite the optimization results reporting that 85% of all generated patterns took less than one minute to be computed, the exhaustive search as well as the search space exploration without assistive automation are major obstacles for application of the method by clinicians. Whereas the exhaustive search is partially addressed in this work by concluding that better designs feature a higher number of cuts $\zeta$, elllipses in $\mathbb{S}$ distributed equidistantly and low polygon degrees $n$, the automation of the search is not resolved here. An interactive design approach could be developed offering the user to modify the orthosis slightly by changing one parameter at a time and generating a new pattern. The procedure could be repeated until a satisfying orthosis is generated. The produced prototype shows satisfying preliminary results and verified the potential of applying origami to develop an alternative to plaster casts. The investigation of how generated designs and their performance are sensitive to different weight factors, application of more advanced scanning procedures for data acquisition, automating the design selection, as well as the improvement of the generation method are left for the future work.

## References

Cai, J., Deng, X., Feng, J., and Zhou, Y. (2015), "Geometric design and mechanical behavior of a deployable cylinder with Miura origami", *Smart Materials and Structures*, Vol. 24 No. 12, p. 125031, https://doi.org/10.1088/0964-1726/24/12/125031

Chen, Y., Feng, H., Ma, J., Peng, R., and You, Z. (2016), "Symmetric waterbomb origami", *Proceedings of the Royal Society A: Mathematical, Physical and Engineering Sciences*, Vol. 472 No. 2190, p. 20150846, https://doi.org/10.1098/rspa.2015.0846



https://doi.org/10.1017/pds.2022.125 Published online by Cambridge University Press

Chen, Y., Lin, H., Zhang, X., Huang, W., Shi, L., and Wang, D. (2017), "Application of 3D-printed and patient-specific cast for the treatment of distal radius fractures: initial experience", *3D Printing in Medicine*, Vol. 3 No. 1, pp. 1-9, https://dx.doi.org/10.1186%2Fs41205-017-0019-y

Demaine, E.D. and Tachi, T., (2017), "Origamizer: A practical algorithm for folding any polyhedron", *In 33rd International Symposium on Computational Geometry, Schloss Dagstuhl-Leibniz-Zentrum fuer Informatik*.

De Souza, M.A., Schmitz, C., Pinhel, M.M., Setti, J. A.P., and Nohama, P. (2017), "Proposal of custom made wrist orthoses based on 3D modelling and 3D printing", 2017 *39th Annual International Conference of the IEEE Engineering in Medicine and Biology Society, Jeju Island, South Korea, July 11-15*, IEEE, Parana, pp. 3789-3792, https://doi.org/10.1109/embc.2017.8037682

Dieleman, P., Vasmel, N., Waitukaitis, S., van Hecke, M. (2020), "Jigsaw puzzle design of pluripotent origami", *Nat. Phys.*, Vol. 16, pp. 63–68, https://doi.org/10.1038/s41567-019-0677-3

Dudte, L.H., Vouga, E., Tachi, T., and Mahadevan, L. (2016), "Programming curvature using origami tessellations", *Nature Materials*, Vol. 15, No. 5, pp. 583-588, https://doi.org/10.1038/nmat4540

Dudte, L.H., Choi, G.P.T., and Mahadevan, L. (2021), "An additive algorithm for origami design", *Proc. Natl. Acad. Sci.*, Vol., 118, No. 21, p. e2019241118, https://doi.org/10.1073/pnas.2019241118

Francis, K.C., Rupert, L.T., Lang, R.J., Morgan, D.C., Magleby, S.P. and Howell, L.L. (2014). "From crease pattern to product: considerations to engineering origami-adapted designs" *In International Design Engineering Technical Conferences and Computers and Information in Engineering Conference*, Vol. 46377, p. V05BT08A030, https://doi.org/10.1115/DETC2014-34031

Kim, H. and Jeong, S. (2015), "Case study: Hybrid model for the customized wrist orthosis using 3D printing", *Journal of Mechanical Science and Technology*, Vol. 29, No. 12, pp. 5151-5156, https://doi.org/10.1007/s12206-015-1115-9

Lang, R.J. (2017), *Twists, Tilings, and Tessellations: Mathematical Methods for Geometric Origami*. CRC Press, Taylor & Francis Group, Boca Raton, https://doi.org/10.1201/9781315157030

Lang, R.J., Tolman, K.A., Crampton, E.B., Magleby, S.P., and Howell, L.L. (2018), "A review of thickness-accommodation techniques in origami-inspired engineering", *Applied Mechanics Reviews*, Vol. 70 No. 1p. 010805, https://doi.org/10.1115/1.4039314

Li, J., and Tanaka, H. (2018a), "Feasibility study applying a parametric model as the design generator for 3D--printed orthosis for fracture immobilization", *3D Printing in Medicine*, Vol. 4 No. 1, pp. 1-15, https://doi.org/10.1186/s41205-017-0024-1

Li, J., and Tanaka, H. (2018b), "Rapid customization system for 3D-printed splint using programmable modeling technique--a practical approach", *3D Printing in Medicine*, Vol. 4 No. 1, pp. 1-21, https://doi.org/10.1186/s41205-018-0027-6

Lin, H., Shi, L., and Wang, D. (2016), "A rapid and intelligent designing technique for patient-specific and 3D-printed orthopedic cast", *3D Printing in Medicine*, Vol. 2 No. 1, pp. 1-10, https://doi.org/10.1186/s41205-016-0007-7

Meloni, M., Cai, J., Zhang, Q., Sang-Hoon Lee, D., Li, M., Ma, R., Parashkevov, T.E. and Feng, J. (2021) "Engineering Origami: A Comprehensive Review of Recent Applications, Design Methods, and Tools", *Advanced Science*, Vol. 8, No. 13, pp. 2000636, https://doi.org/10.1002/advs.202000636

Miura, K. (1985), "Method of packaging and deployment of large membranes in space", *The Institute of Space and Astronautical Science Report*, No. 618, pp. 1-9

Qlone (2017), *Qlone*, Available at: https://www.qlone.pro/ (accessed 04.08.2021).

Tang, J. M., Tian, M. Q., Wang, C. J., Wang, X. S., and Mao, H. L. (2021), "A novel scheme of folding discretized surfaces of revolution inspired by waterbomb origami", *Mechanism and Machine Theory*, Vol. 165, p. 104431, https://doi.org/10.1016/j.mechmachtheory.2021.104431

Yoshimura, Y. (1951), On the mechanism of a circular cylindrical shell under axial compression, Technical Report NACA-TM-1390, NACA Technical Reports, USA, https://digital. library. unt. edu/ark:/67531/metadc62872

Yu, Y., Hong, T.C.K., Economou, A., and Paulino, G.H. (2021). "Rethinking Origami: A Generative Specification of Origami Patterns with Shape Grammars", *Computer-Aided Design*, Vol. 137, p. 103029, https://doi.org/10.1016/j.cad.2021.103029

Zimmermann, L., Shea, K., and Stankovic, T. (2020), "Conditions for Rigid and Flat Foldability of Degree-*n* Vertices in Origami", *Journal of Mechanisms and Robotics*, Vol. 12 No. 1, p. 011020, https://doi.org/10.1115/1.4045249

Zimmermann, L., Shea, K., and Stankovic, T. (2022), "A Computational Design Synthesis Method for the Generation of Rigid Origami Crease Patterns", *Journal of Mechanisms and Robotics*, Vol. 14, No. 3, p. 031014, https://doi.org/10.1115/1.4052847

Zirbel, S.A., Lang, R.J., Thomson, M.W., Sigel, D.A., Walkemeyer, P.E., Trease, B.P., Magleby, S.P. and Howell, L.L. (2013), "Accommodating thickness in origami-based deployable arrays", *Journal of Mechanical Design*, Vol. 135, No. 11, p. 111005, https://doi.org/10.1115/1.4025372



https://doi.org/10.1017/pds.2022.125 Published online by Cambridge University Press